Journal of Applied Geophysics 107 (2014) 188–194

Contents lists available at ScienceDirect

Journal of Applied Geophysics

journal homepage: www.elsevier.com/locate/jappgeo

The application of extended Euler deconvolution method in the interpretation of potential field data

Guoqing Ma

College of Geoexploration Science and Technology, Jilin University, Changchun, China

ARTICLE INFO

Article history:
Received 30 April 2014
Accepted 2 June 2014
Available online 9 June 2014

Keywords:
Extended Euler deconvolution
Horizontal derivative
Vertical derivative
Location

ABSTRACT

Euler deconvolution method is a usually used automatic method in the interpretation of potential field data, and we all know that the precision of the inversion results depends on the difference between the given structural index and the true shape. Extended Euler deconvolution methods can remove the interference of structural index, which use the derivatives of potential field data to compute the location parameters. However, we discover some rules in the application of extended Euler deconvolution method to interpret potential field data. First, single horizontal derivative cannot obtain the source locations correctly, but the combinations of horizontal derivatives can estimate the location parameters effectively. When using the functions of vertical derivative to interpret the potential field data that exist positive and negative anomalies simultaneously, the inversion results will produce additional results, but the matrix or function composed of the horizontal derivatives will not have additional results, and we also find that the results computed by the matrix composed of the horizontal derivatives are insensitive to noise. Applying the extended Euler deconvolution method to interpret real potential field data, we also find that the matrix composed by the horizontal derivatives can ascertain the location parameters of the sources more correctly.

1. Introduction

Euler deconvolution (Reid et al., 1990; Thompson, 1982) is a popularly used automatic interpretation method of potential field data, which uses the original anomaly, its derivatives and the given structural index to estimate the source location parameters, and the precision of the estimated locations depends on the similarity between the given structural index and the real shape (Barbosa et al., 1999; Ravat, 1994; Stavrev, 1997). In order to reduce the interference of structural index, many people (FitzGerald et al., 2004; Gerovska and Arauzo-Bravo, 2003; Hsu, 2002; Huang et al., 1995; Mushayandebvu et al., 2001; Salem and Ravat, 2003) presented extended Euler deconvolution methods, which use the derivatives of potential field data to compute the locations of the sources. Because the derivatives of potential field data can lower the amplitude of the background field, the structural index can be calculated. Some people (Ma, 2013; Salem et al., 2008; Thurston and Smith, 1997) use the ratios between derivatives to compute the source locations, and these methods can balance the amplitude of the anomalies generated by the sources with different depths, which can discover weak anomalies more effectively.

In my study, I find that there are some notable problems in the application of extended Euler deconvolution method. Single horizontal derivative cannot estimate the locations of the sources correctly, and the results computed by the vertical derivatives will produce additional results in some cases, and are sensitive to noise, but the results computed by the matrix composed of the horizontal derivatives are more accurate and stable.

1.1. Extended Euler deconvolution method

The conventional Euler deconvolution method (Reid et al., 1990; Thompson, 1982) can be given by

$$(x-x_0)\frac{\partial f}{\partial x}+(y-y_0)\frac{\partial f}{\partial y}+(z-z_0)\frac{\partial f}{\partial z}=-N(f-B) \quad (1)$$

where, f is the original potential field data, x, y and z are the known observation coordinates of points, x_0, y_0, and z_0 are the unknown source coordinates, B is the background field, and N is the structural index, which delineates the nature of the source (Reid et al., 1990; Stavrev, 1997).

Depending on Eq. (1) we can see that the solution of Euler equation requires the information about the structural index of the source, but the structural index is not unique and is hard to know for an unknown area. In order to avoid the interference of structural index, many people (FitzGerald et al., 2004; Gerovska and Arauzo-Bravo, 2003; Hsu, 2002; Huang et al., 1995) presented extended Euler deconvolution methods, which use the derivatives of potential field data to compute the location

E-mail address: maguoqing@jlu.edu.cn.

http://dx.doi.org/10.1016/j.jappgeo.2014.06.002
0926-9851/

parameters. Assuming the background field B as a constant value, and the derivatives of Eq. (1) In the x, y and z directions can be expressed as

$$(x-x_0)\frac{\partial^2 f}{\partial x^2}+(y-y_0)\frac{\partial^2 f}{\partial x\partial y}+(z-z_0)\frac{\partial^2 f}{\partial x\partial z}=-(N+1)\frac{\partial f}{\partial x} \tag{2}$$

$$(x-x_0)\frac{\partial^2 f}{\partial x\partial y}+(y-y_0)\frac{\partial^2 f}{\partial y^2}+(z-z_0)\frac{\partial^2 f}{\partial y\partial z}=-(N+1)\frac{\partial f}{\partial y} \tag{3}$$

$$(x-x_0)\frac{\partial^2 f}{\partial x\partial z}+(y-y_0)\frac{\partial^2 f}{\partial y\partial z}+(z-z_0)\frac{\partial^2 f}{\partial z^2}=-(N+1)\frac{\partial f}{\partial z} \tag{4}$$

We can use one of Eqs (2)–(4) to compute the location parameters of the sources without the priori information about the structural index. Some people use the functions of the derivatives to finish this work (Huang et al., 1995; Ma et al, 2013), such as total horizontal derivative (THD), analytic signal (AS), normalized horizontal tilt angle (TDX) et al., and the corresponding expressions can be written by

$$(x-x_0)\frac{\partial THD}{\partial x}+(y-y_0)\frac{\partial THD}{\partial y}+(z-z_0)\frac{\partial THD}{\partial z}=-(N+1)THD \tag{5}$$

$$(x-x_0)\frac{\partial AS}{\partial x}+(y-y_0)\frac{\partial AS}{\partial y}+(z-z_0)\frac{\partial AS}{\partial z}=-(N+1)AS \tag{6}$$

$$(x-x_0)\frac{\partial TDX}{\partial x}+(y-y_0)\frac{\partial TDX}{\partial y}+(z-z_0)\frac{\partial TDX}{\partial z}=0 \tag{7}$$

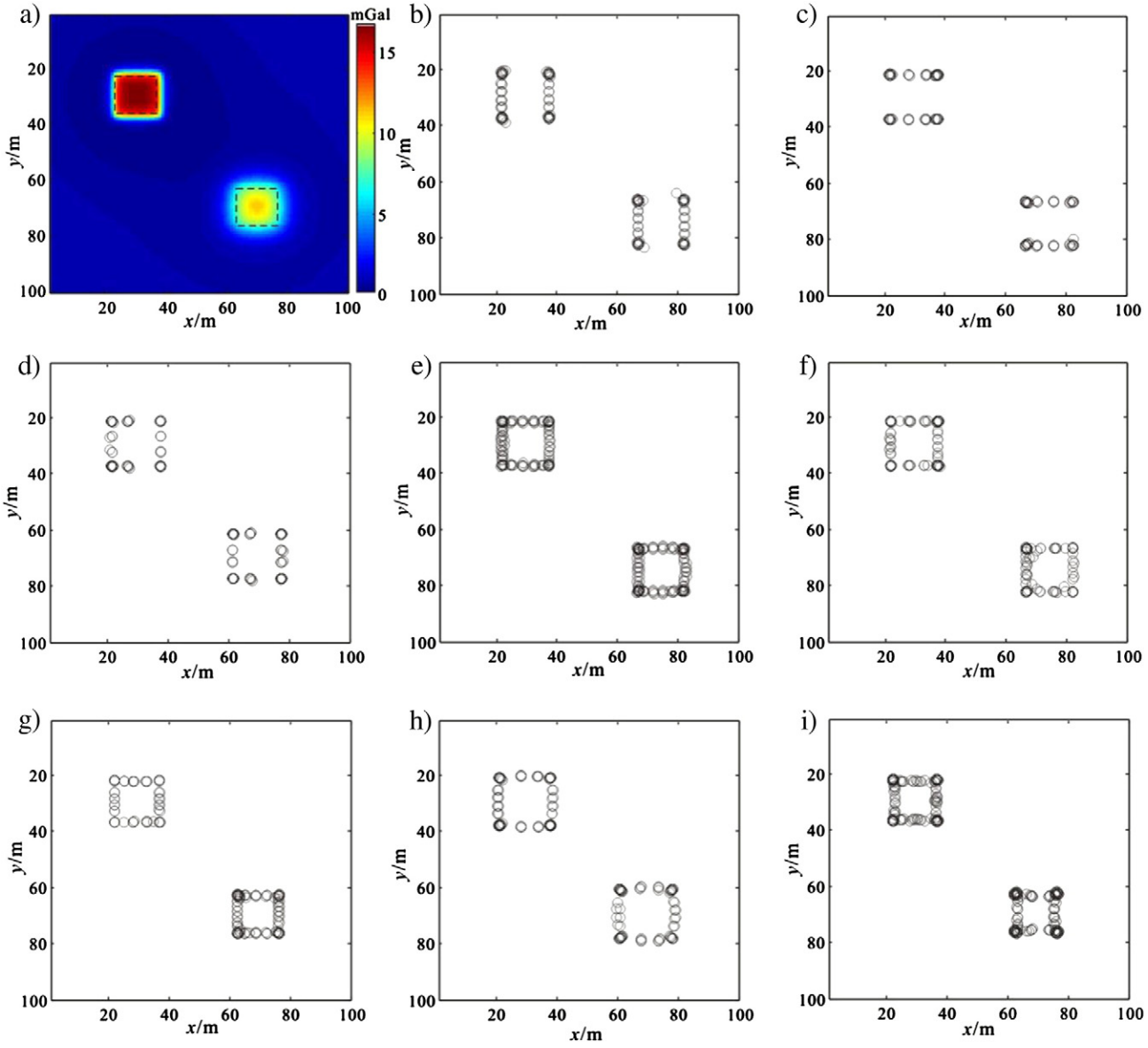

Fig. 1. (a) Synthetic gravity anomaly generated by two identical rectangular prisms with depths of 10 and 15 m. (b) Estimated horizontal locations computed by Eq. (2). (c) Estimated horizontal locations computed by Eq. (3). (d) Estimated horizontal locations computed by Eq. (4). (e) Estimated horizontal locations computed by the matrix composed of Eqs. (2) and (3). (f) Estimated horizontal locations computed by Eq. (5). (g) Estimated horizontal locations computed by the matrix composed of Eqs (2)–(4). (h) Estimated horizontal locations computed by Eq. (6). (i) Estimated horizontal locations computed by Eq. (7).

where, $THD = \sqrt{\left(\frac{\partial f}{\partial x}\right)^2 + \left(\frac{\partial f}{\partial y}\right)^2}$, $AS = \sqrt{\left(\frac{\partial f}{\partial x}\right)^2 + \left(\frac{\partial f}{\partial y}\right)^2 + \left(\frac{\partial f}{\partial z}\right)^2}$ and $TDX = \operatorname{atan}\left(\frac{\sqrt{\left(\frac{\partial f}{\partial x}\right)^2 + \left(\frac{\partial f}{\partial y}\right)^2}}{\frac{\partial f}{\partial z}}\right)$. We also can use one of Eqs. (5)–(7) to compute the source locations without the information about the nature of the source.

1.2. Tests on synthetic potential field data

In order to show the application effect of extended Euler deconvolution method, I compared the inversion results computed by different equations. Fig. 1a shows synthetic gravity anomaly generated by two prisms with depths of 10 and 15 m, respectively. Applying the above extended Euler deconvolution methods to compute the source location parameters, and the size of the window is 5×5. I use a simple selection criterion to get better results, and the criterion is that the distance between the center of the window and the estimated location is smaller than the size of the window. Fig. 1b and c shows the estimated horizontal locations of the sources computed by Eqs. (2) and (3) respectively, and we can see that the horizontal derivatives of the Euler deconvolution only can obtain the edges of the opposite directions. Fig. 1d shows the locations of the sources computed by Eq. (3), and the estimated horizontal locations can delineate the edges of the sources correctly, so the vertical derivatives of the conventional Euler equation can be directly used to estimate the source locations. Fig. 1e shows the horizontal locations of the sources estimated by the matrix composed by Eqs. (2) and (3), and Fig. 1f shows the estimated locations by Eq. (5). The results computed by the matrix composed of horizontal derivatives are more accurate than the results computed by the THD.

Fig. 1g shows the horizontal locations of the sources estimated by the matrix composed of Eqs. (2)–(4), and Fig. 1h and i show the estimated locations of the sourced by Eqs. (6) and (7), respectively. Depending on the results we can deduce that the precision of the results computed by the matrix composed of different derivatives is higher than the results computed by the functions of the derivatives.

Fig. 2a shows the histogram of depth estimated using Eq. (4), and Fig. 2b shows the histogram of the depth estimated by the matrix composed of Eqs. (2) and (3). Fig. 2c shows the depth computed by Eq. (5). We can see that the estimated depth by different methods are both close to real depths, and the results computed by the matrix composed of horizontal derivatives are more accurate than the results computed by the sum of squares of horizontal derivatives and vertical derivative. Fig. 2d shows the depth computed by the matrix composed of Eqs. (2)–(4), and Fig. 2e and f show the depth computed by Eqs. (6) and (7), respectively. We can find that the results computed by the matrix composed of all the derivatives are consistent with the true depths totally, and are mostly precise.

In the interpretation of real potential field data, the data often contains the positive and negative anomalies together. Fig. 3a shows synthetic gravity anomaly generated by two prisms with depths of 10 and 15 m, and their densities are $+1$ and -1 g/cm^3, respectively. Fig. 3b and c show the estimated horizontal locations of the sources by Eqs. (2) and (3) respectively, and the results can show the edges of the opposite directions. Fig. 3d shows the estimated horizontal locations of the sources by Eq. (4), and we can see that the inversion results produce additional results between the anomalies, so we cannot individually use the vertical derivative to estimate the locations of the sources in this case. Fig. 3e shows the horizontal locations of the sources estimated by the matrix composed of Eqs. (2) and (3), and Fig. 3f shows the estimated locations by Eq. (5). The results computed by the matrix composed of horizontal derivatives are more accurate than the results computed by the THD, and both don't have the additional results.

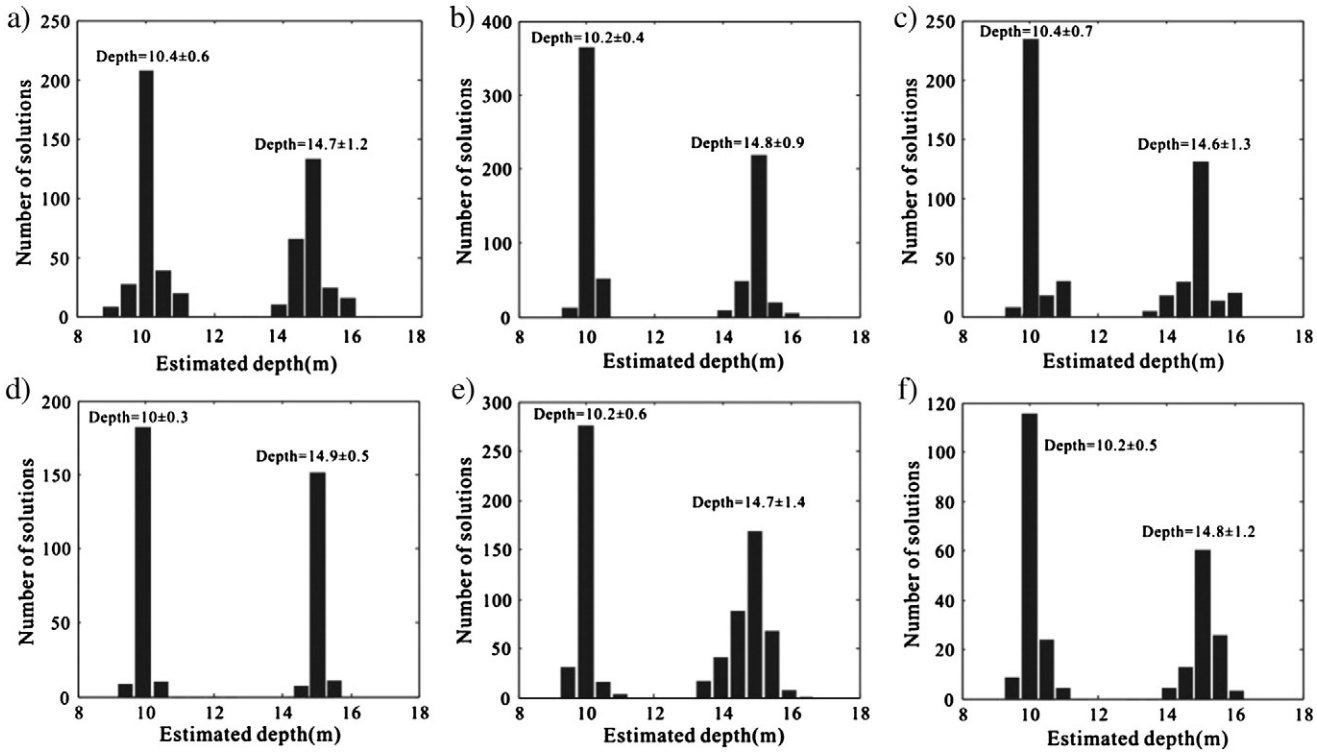

Fig. 2. (a) Histogram of the depths estimated by Eq. (4). (b) Histogram of the depths estimated by the matrix composed of Eqs. (2) and (3). (c) Histogram of the depths estimated by Eq. (5). (d) Histogram of the depths estimated by the matrix composed of Eqs (2)–(4). (e) Histogram of the depths estimated by Eq. (6). (f) Histogram of the depths estimated by Eq. (7).

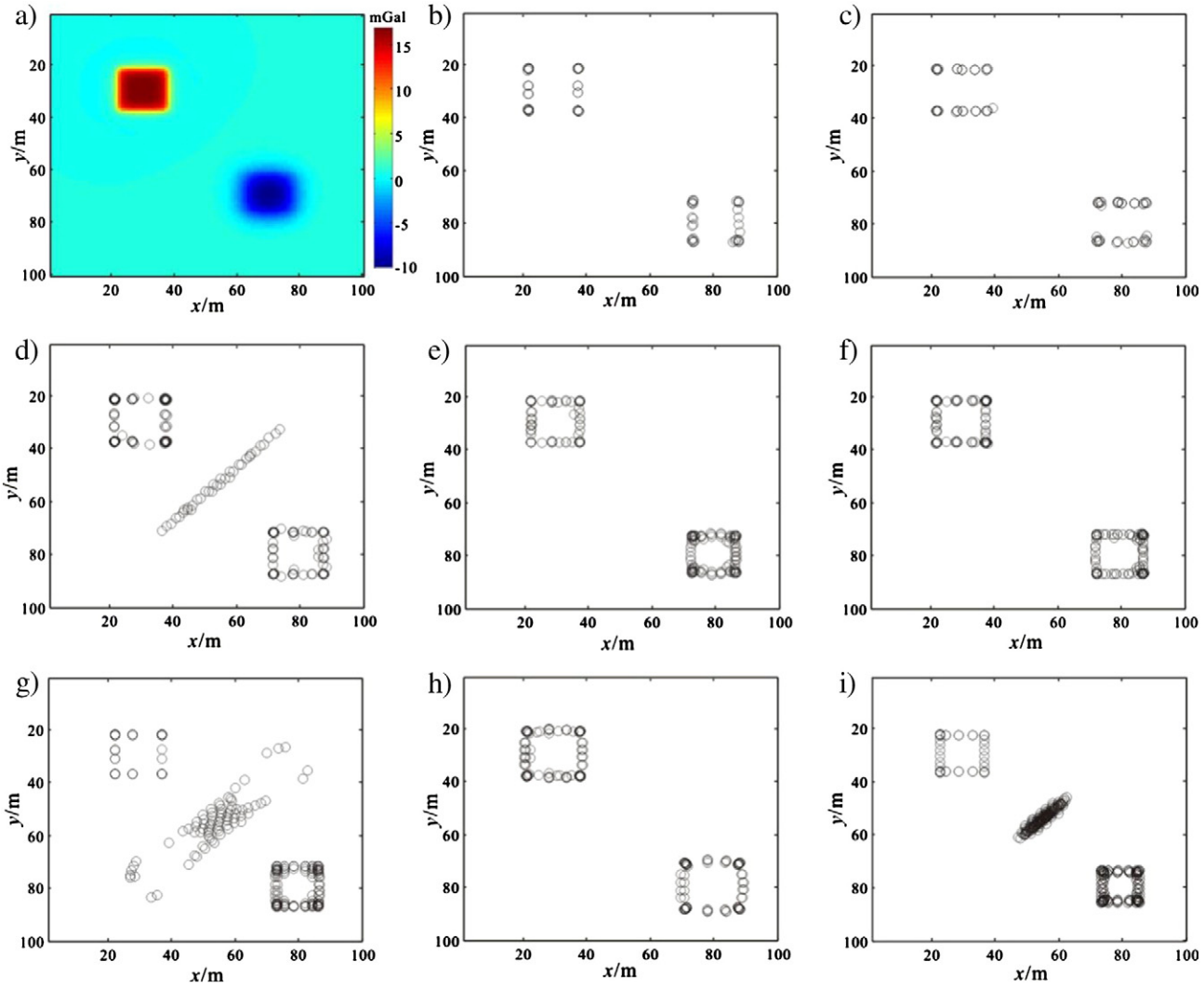

Fig. 3. (a) Synthetic gravity anomaly generated by two prisms, and their densities are +1 and −1 g/cm^3. (b) Estimated horizontal locations computed by Eq. (2).(c) Estimated horizontal locations computed by Eq. (3). (d) Estimated horizontal locations computed by Eq. (4). (e) Estimated horizontal locations computed by the matrix composed Eqs. (2) and (3). (f) Estimated horizontal locations computed by Eq. (5). (g) Estimated horizontal locations computed by the matrix composed of Eqs (2)–(4). (h) Estimated horizontal locations computed by Eq. (6). (i) Estimated horizontal locations computed by Eq. (7).

Fig. 3g shows the horizontal locations of the sources estimated by the matrix composed of Eqs. (2) and (4), and Fig. 2h and i show the estimated locations of the sourced by Eqs. (6) and (7), respectively. We can see that the results computed by the analytic signal do not have additional results, and the other two methods produce the additional results. The possible reason is that the vertical derivative over the source edges is equal to zero, and the vertical derivative between the positive and negative anomalies is also zero, so the inversion results will produce additional results. The value of the TDX depends on the zero of the vertical derivative, so the results estimated by the TDX also have the additional results. Depending on the results we know that we cannot use vertical derivative to interpret real potential field data, and should use the matrix composed of the horizontal derivatives to estimate the locations of the sources.

In the interpretation of real potential field data, the noise is a considerable factor. We added the Gaussian noise with SNR (Signal Noise Ratio) of 50 into the gravity anomaly in Fig. 1a. Fig. 4a shows the noise-corrupted gravity anomaly. The results estimated by Eqs. (2) and (3) are shown in Fig. 4b and c, respectively, and the inversion results are still stable, but the results cannot finish the interpretation of gravity anomaly effectively. Fig. 4d shows the results estimated by Eq. (4), and we can see that the edges delineated by the inversion results are distorted, so the vertical derivatives are more sensitive to noise. Fig. 4e shows the results estimated by the matrix composed of Eqs. (2) and (3), and the results can delineate the locations of the sources correctly. The results computed by Eq. (5) are shown in Fig. 4f. Fig. 4g shows the results computed by the matrix composed of Eqs. (2), (3) and (4), and the estimated horizontal locations are consistent with the true locations of the sources. Fig. 4h and i show the locations of the sources estimated by Eqs. (6) and (7), and the TDX can obtain accurate results. Depending on the results we can deduce that the matrix composed of the derivatives can obtain more accurate results, and can lower the interference of noise.

Fig. 5a shows the histogram of depth estimated by Eq. (4) for noise-corrupted data, and we can see that the precision of the depth is reduced because of the effect of noise. Fig. 5b shows the histogram of the depth estimated by the matrix composed of Eqs. (2) and (3), and Fig. 5c shows the depth estimated by Eq. (5). We can see that the estimated depth by the horizontal derivatives is still close to real depth, and is insensitive to

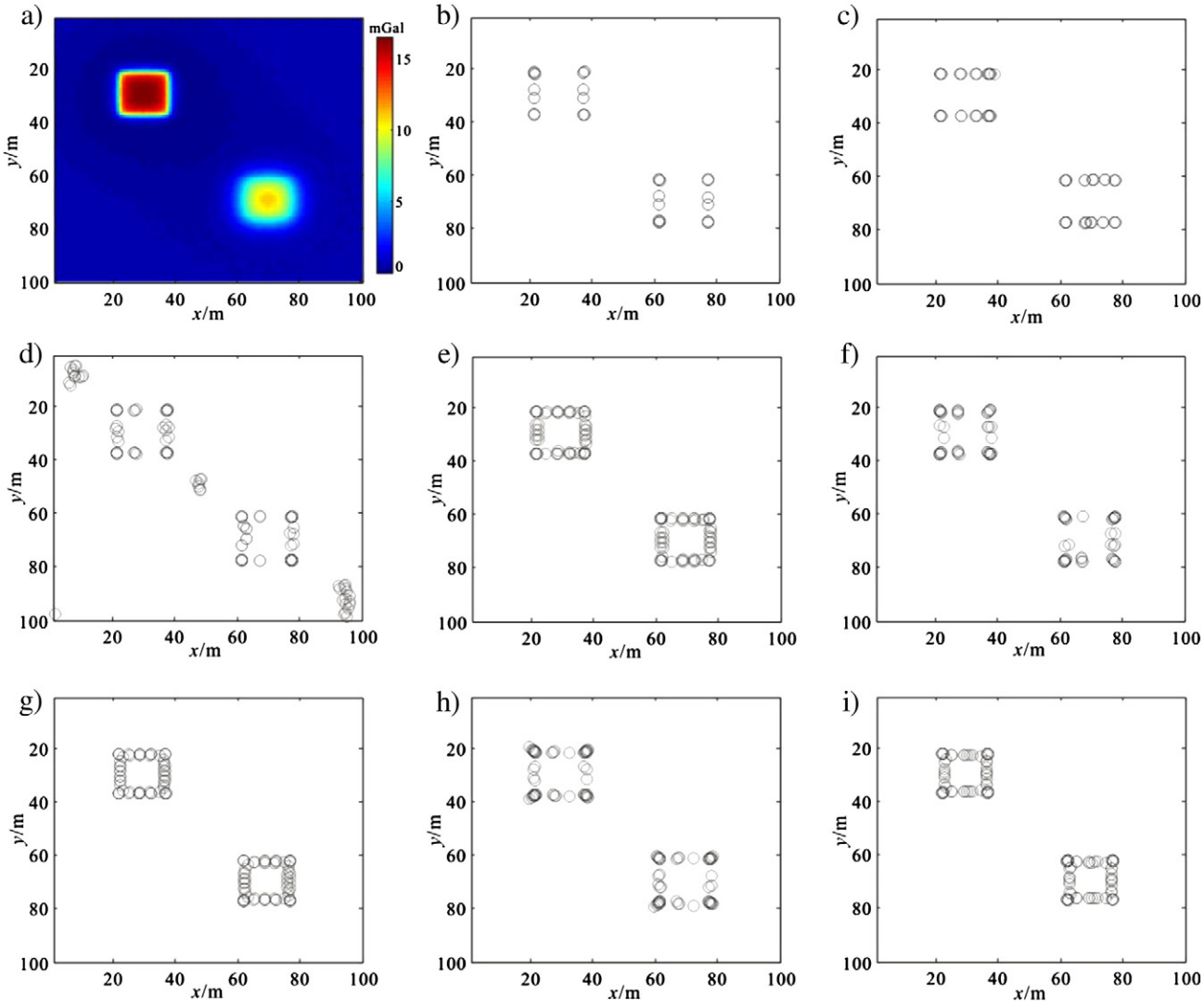

Fig. 4. (a) Noise-corrupted gravity anomaly. (b) Estimated horizontal locations computed by Eq. (2).(c) Estimated horizontal locations computed by Eq. (3). (d) Estimated horizontal locations computed by Eq. (4). (e) Estimated horizontal locations computed by the matrix composed of Eqs. (2) and (3). (f) Estimated horizontal locations computed by Eq. (5). (g) Estimated horizontal locations computed by the matrix composed of Eqs (2)–(4). (h) Estimated horizontal locations computed by Eq. (6). (i) Estimated horizontal locations computed by Eq. (7).

noise. Fig. 5d shows the depth computed by the matrix composed of Eqs. (2) and (4), and Fig. 5e and f show the depth computed by Eqs. (6) and (7), respectively. We can find that the precision of the depth computed by the functions of vertical derivative is reduced seriously.

We synthetically consider the feature of anomalies and the interference of noise, and we should use the matrix composed of horizontal derivatives to estimate the location parameters of the sources.

1.3. Application to real gravity anomaly

Fig. 6a shows the measured gravity anomaly of Luzong area, south of China. Fig. 6b shows the estimated location parameters of Eq. (4), and the size of the circle is proportional to the depth, and the range of the depth is from 240 m to 610 m. Fig. 6c shows the locations of the sources computed by the matrix composed of Eqs. (2) and (3). We can see that the results computed by the horizontal derivatives are relatively concentrated, and the results computed by the vertical derivative contain many additional results, such as the area marked by the white circle in Fig. 6a. The results computed by THD are shown in Fig. 6d. Fig. 6e shows the results computed by the matrix composed of the horizontal derivatives and vertical derivative, and Fig. 6f shows the results computed by the TDX. We know that the vertical derivatives are more sensitive to noise, so the results computed by the TDX are relative divergent.

2. Conclusions

In this paper, I discuss the application way of extended Euler deconvolution method in the interpretation of potential field data.<!——> I demonstrate that we cannot individually use single horizontal derivative to estimate the source locations, and the vertical derivative is sensitive to noise, and when using the vertical derivative to interpret the data that contains positive and negative anomalies simultaneously, this will produce additional results. The

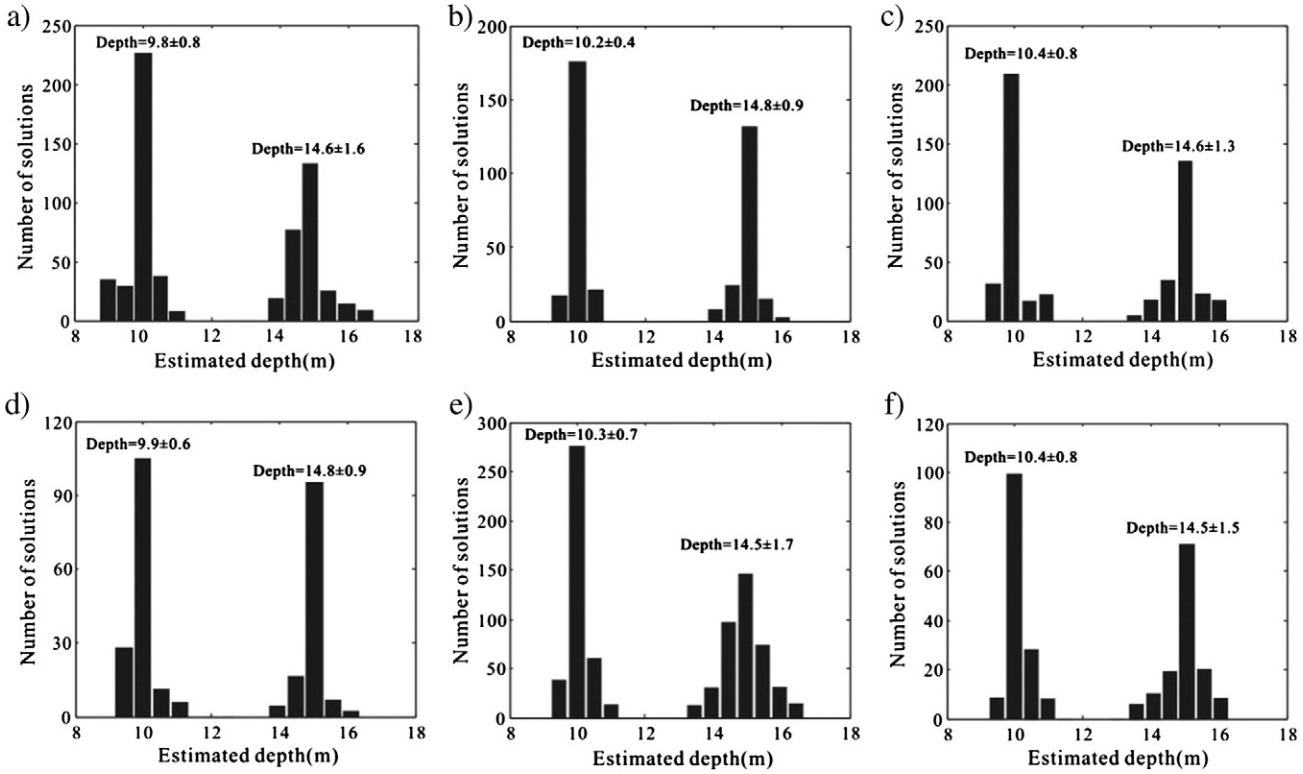

Fig. 5. (a) Histogram of the depths estimated by Eq. (4). (b) Histogram of the depths estimated by the matrix composed of Eqs. (2) and (3). (c) Histogram of the depths estimated by Eq. (5). (d) Histogram of the depths estimated by the matrix composed of Eqs. 2–4. (e) Histogram of the depths estimated by Eq. (6). (f) Histogram of the depths estimated by Eq. (7).

results show that the matrix composed of horizontal derivatives can obtain more accurate results, and are more insensitive to noise, so we should use the matrix composed of the horizontal derivatives to compute the location parameters.

Acknowledgment

This work is supported by China Postdoctoral Science Foundation (2014M550173).

References

Barbosa, V.C.F., Silva, J.B.C., Medeiros, W.E., 1999. Stability analysis and improvement of structural index estimation in Euler deconvolution. Geophysics 64, 48–60.

FitzGerald, D., Reid, A., McInerney, P., 2004. New discrimination techniques for Euler deconvolution. Comput. Geosci. 30, 461–469.

Gerovska, D., Arauzo-Bravo, M.J., 2003. Automatic interpretation of magnetic data based on Euler deconvolution with unprescribed structural index. Comput. Geosci. 29, 949–960.

Hsu, S.K., 2002. Imaging magnetic sources using Euler's equation. Geophys. Prospect. 50, 15–25.

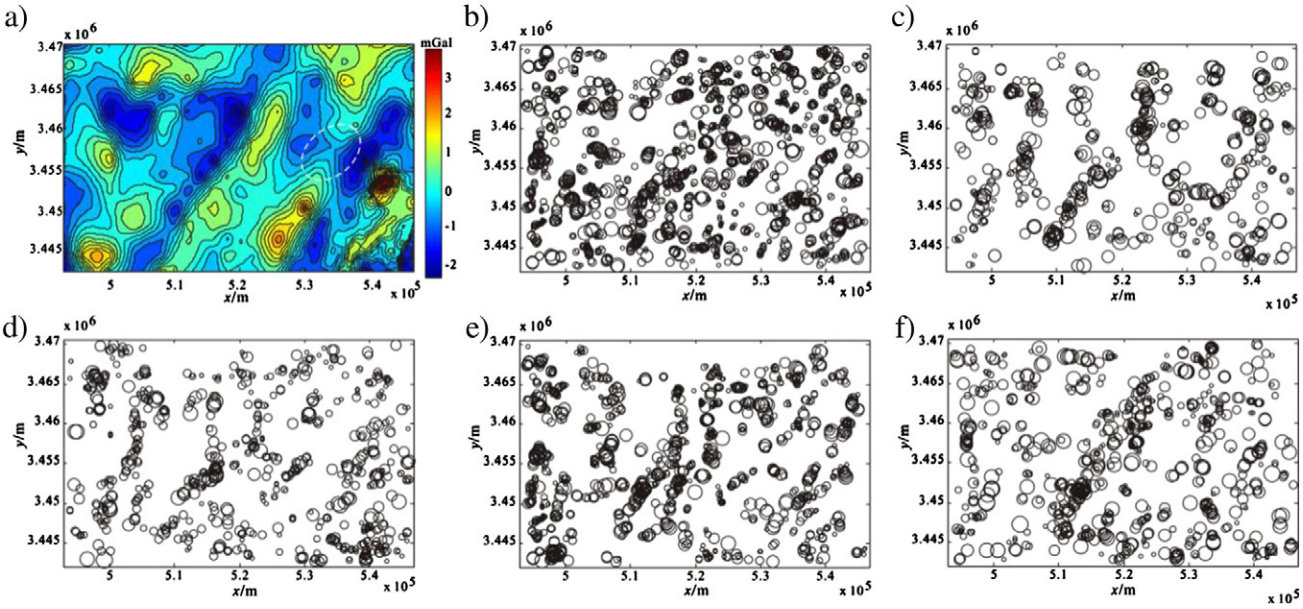

Fig. 6. (a) Measured gravity anomaly of Luzong area. (b) Estimated horizontal locations computed by Eq. (4). (c) Estimated horizontal locations computed by the matrix composed of Eqs. (2) and (3). (d) Estimated horizontal locations computed by Eq. (5). (e) Estimated horizontal locations computed by the matrix composed of Eqs (2)–(4). (f) Estimated horizontal locations computed by Eq. (7).

Huang, D., Gubbins, D., Clark, R.A., Whaler, K.A., 1995. Combined study of Euler's homogeneity equation for gravity and magnetic field. 57th EAGE conference, Glasgow, UK, Extended Abstracts, p. 144.
Ma, G., 2013. Combination of horizontal gradient ratio and Euler (HGR-EUL) methods for the interpretation of potential field data. Geophysics 78, J53–J60.
Ma, G., Huang, D., Liu, C., 2013. Application of balanced edge detection filters to estimate the location parameters of the causative sources using potential field data. J. Appl. Geophys. 99, 18–23.
Mushayandebvu, M.F., van Driel, P., Reid, A., Fairhead, J.D., 2001. Magnetic source parameters of two-dimensional structures using extended Euler deconvolution. Geophysics 66, 814–823.
Ravat, D., 1994. Use of fractal dimension to determine the applicability of Euler's homogeneity equation for finding source locations of gravity and magnetic anomalies. Proc. of the Symposium on the Application of Geophysics to Engineering and Environmental Problems, Boston, March 1994. Environmental and Engineering Geophysical Society, Englewood, CO, pp. 41–53.
Reid, A.B., Allsop, J.M., Granser, H., Millett, A.J., Somerton, I.W., 1990. Magnetic interpretation in three dimensions using Euler deconvolution. Geophysics 55, 80–91.
Salem, A., Ravat, D., 2003. A combined analytic signal and Euler method (AN-EUL) for automatic interpretation of magnetic data. Geophysics 68, 1952–1961.
Salem, A., Williams, S., Fairhead, D., Smith, R., Ravat, D., 2008. Interpretation of magnetic data using tilt-angle derivatives. Geophysics 73, L1–L10.
Stavrev, P., 1997. Euler deconvolution using differential similarity transformations of gravity or magnetic anomalies. Geophys. Prospect. 45, 207–246.
Thompson, D.T., 1982. EULDPH—a new technique for making computer assisted depth estimates from magnetic data. Geophysics 47, 31–37.
Thurston, J.B., Smith, R.S., 1997. Automatic conversion of magnetic data to depth, dip, and susceptibility contrast using the SPI method. Geophysics 62, 807–813.